

# Minimising Time-Stepping Errors in Numerical Models of the Atmosphere and Ocean



University of Reading

School of Mathematics, Meteorology and Physics

Robert J. Smith

August 2010

---

This dissertation is submitted to the Department of Mathematics and Meteorology in partial fulfilment of the requirements for the degree of Master of Science.

## Abstract

Due to the wide usage of numerical models in Meteorology it is essential reduce model errors to get better predictions. The model errors are due to space and time-differencing. The model errors are considered separately with the main focus of the paper on time-differencing schemes. The Asselin-filtered leapfrog scheme, the proposed modified filters and the Adams-Bashforth family of schemes are employed into an existing nonlinear model QUAGMIRE v1.3. An analysis of each scheme was taken to determine the wave amplitude and associated amplitude error. It was found that all the schemes have problematic amplitude errors, some to a lesser extent than others. The third-order Adams-Bashforth method, albeit more accurate requires more storage requirements. The third-order Adams-Bashforth and Asselin-filtered leapfrog when  $\alpha = 0.5$  have proved to be the preferred methods of choice from the sample of schemes taken. Further study into higher order schemes would be beneficial along with the consideration of multiple layers in the nonlinear model.

## **Acknowledgments**

I would like to thank my supervisor Dr. Paul D. Williams for all his enthusiasm, help and support given whilst completing this project.

## **Declaration**

I confirm that this is my own work, and the use of all material from other sources has been properly and fully acknowledged.

Signature .....

Date .....

# Contents

<b>Abstract</b> . . . . .	i
<b>Acknowledgments</b> . . . . .	ii
<b>Declaration</b> . . . . .	ii
<b>List of Figures</b> . . . . .	vii
<b>List of Tables</b> . . . . .	viii
<b>1 Introduction</b> . . . . .	<b>1</b>
1.1 What are Numerical Models? . . . . .	1
1.2 Sources of Error . . . . .	1
1.3 Aims . . . . .	4
1.4 Outline . . . . .	4
<b>2 Time-Differencing Schemes</b> . . . . .	<b>5</b>
2.1 Leapfrog Scheme . . . . .	5
2.1.1 Leapfrog Scheme with Robert-Asselin Filter . . . . .	6
2.1.2 Leapfrog with Modified Filter . . . . .	7
2.2 Adams-Bashforth Schemes . . . . .	7
2.2.1 First-Order . . . . .	8
2.2.2 Second-Order . . . . .	8
2.2.3 Third-Order . . . . .	8
<b>3 Model Description</b> . . . . .	<b>10</b>
3.1 QUAGMIRE v1.3 . . . . .	10
3.2 Equations . . . . .	11
3.3 Assumptions . . . . .	14

3.4	Initialisation . . . . .	16
<b>4</b>	<b>Numerical Results</b>	<b>18</b>
4.1	Leapfrog with Robert-Asselin Filter . . . . .	18
4.1.1	Standard Filter $\alpha = 1$ . . . . .	18
4.1.2	Modified Filter $\alpha = 0.5$ . . . . .	21
4.1.3	Modified Filter $\alpha = 0$ . . . . .	23
4.2	Adams-Bashforth Schemes . . . . .	25
4.2.1	First-Order . . . . .	25
4.2.2	Second-Order . . . . .	26
4.2.3	Third-Order . . . . .	27
4.3	Deriving Amplitude Errors . . . . .	28
4.4	Combined Leapfrog and Forward Step . . . . .	31
<b>5</b>	<b>Sensitivity Tests</b>	<b>33</b>
5.1	Changes in $\Delta t$ . . . . .	33
5.2	Advection, Forcing and Dissipation . . . . .	34
<b>6</b>	<b>Conclusion</b>	<b>37</b>
6.1	Summary . . . . .	37
6.2	Future Work . . . . .	40
	<b>Bibliography</b> . . . . .	<b>41</b>

# List of Figures

1.1	Comparison between the (a) zonal-mean zonal wind error (m/s) using the leapfrog scheme, (b) zonal-mean zonal wind error (m/s) using the second-order Adams-Bashforth scheme, (c) temperature error using the leapfrog scheme and (d) temperature error using the second-order Adams-Bashforth method. Taken from [9]. . . . .	3
2.1	Comparison between the (a) the standard Robert-Asselin filter and (b) proposed modified filters. Taken from [7]. . . . .	7
3.1	Two layer diagram showing the interface between the two layers where waves will amplify and decay in the QUAGMIRE v1.3 model. . . . .	11
3.2	Shows the grid points across mid-latitudes, where the model fluid flows are solved. There are 16 grid points in the latitudinal direction and 96 in the longitudinal direction equating to grid points every $4^\circ$ of latitude and $2^\circ$ of longitude. . . . .	14
3.3	Shows the amplitude of the perturbation between the two layers in the model for $\Delta t = 0.0008$ using a leapfrog scheme with Robert-Asselin filter of 0.01. . . . .	17
3.4	Shows the perturbations in streamfunction for the upper layer at time 800. . . . .	17
4.1	Leapfrog scheme with standard Robert-Asselin filter for a range of different filter parameters. Shows the amplitude of the perturbation between the two layers in the model for $\alpha = 1$ . . . . .	19

4.2	Leapfrog scheme with standard Robert-Asselin filter for a range of different filter parameters. Shows the amplitude of the perturbation between the two layers relative to the base amplitude for $\alpha = 1$ . The base amplitude being for the filter parameter $\nu = 0.01$ . . . . .	20
4.3	Leapfrog scheme with standard Robert-Asselin filter for a range of different filter parameters with $\alpha = 1$ . Shows the final amplitude versus the filter parameter $\nu$ . . . . .	20
4.4	Leapfrog scheme with modified Robert-Asselin filter for a range of different filter parameters. Shows the amplitude of the perturbation between the two layers in the model for $\alpha = 0.5$ . . . . .	21
4.5	Leapfrog scheme with standard Robert-Asselin filter for a range of different filter parameters. Shows the amplitude of the perturbation between the two layers relative to the base amplitude for $\alpha = 0.5$ . The base amplitude being for the filter parameter $\nu = 0.01$ . . . . .	22
4.6	Leapfrog scheme with standard Robert-Asselin filter for a range of different filter parameters with $\alpha = 0.5$ . Shows the final amplitude versus the filter parameter $\nu$ . . . . .	22
4.7	Leapfrog scheme with modified Robert-Asselin filter for a range of different filter parameters. Shows the amplitude of the perturbation between the two layers in the model for $\alpha = 0$ . . . . .	23
4.8	Leapfrog scheme with standard Robert-Asselin filter for a range of different filter parameters. Shows the amplitude of the perturbation between the two layers relative to the base amplitude for $\alpha = 0$ . The base amplitude being for the filter parameter $\nu = 0.01$ . . . . .	24
4.9	Leapfrog scheme with standard Robert-Asselin filter for a range of different filter parameters with $\alpha = 0$ . Shows the final amplitude versus the filter parameter $\nu$ . . . . .	24
4.10	First-order Adams-Bashforth scheme. Shows the amplitude of the perturbation between the two layers in the model. . . . .	25
4.11	Second-order Adams-Bashforth scheme. Shows the amplitude of the perturbation between the two layers in the model for increasing $\Delta t$ . .	26
4.12	Third-order Adams-Bashforth scheme. Shows the amplitude of the perturbation between the two layers in the model for increasing $\Delta t$ . .	27

4.13	Combined leapfrog and forward step. $N - 1$ leapfrogs to 1 forward step. Shows the amplitude of the perturbation between the two layers in the model. . . . .	32
4.14	Combined leapfrog and forward step. Shows the final amplitude vs $N$ . . . . .	32
5.1	Leapfrog scheme with Robert-Asselin filter for the three cases $\alpha = 1$ , $\alpha = 0.5$ and $\alpha = 0$ . Shows the final amplitude of the perturbation between the two layers in the model for increasing $\Delta t$ . . . . .	34
5.2	Leapfrog scheme with Robert-Asselin filter for the three cases $\alpha = 1$ , $\alpha = 0.5$ and $\alpha = 0$ with a filter parameter $\nu = 0.01$ . Shows the amplitude of the perturbation between the two layers in the model with no advection. Only forcing and dissipation being applied. . . . .	35
5.3	Leapfrog scheme with Robert-Asselin filter for the three cases $\alpha = 1$ , $\alpha = 0.5$ and $\alpha = 0$ with a filter parameter $\nu = 0.01$ . Shows the amplitude of the perturbation between the two layers in the model with no forcing and dissipation. Only advection being applied. . . . .	35
6.1	Shows the comparison of the results from the Adams-Bashforth second-order, Adams-Bashforth third-order and the leapfrog scheme with Robert-Asselin filter for the three cases of $\alpha$ . Shows the amplitude of the perturbation between the two layers in the model for $\Delta t = 0.0008$ . . . . .	38
6.2	Shows the comparison of the results from the Adams-Bashforth second order, Adams-Bashforth third order and the leapfrog scheme with Robert-Asselin filter for the three cases of $\alpha$ . Shows the amplitude of the perturbation between the two layers in the model for $5\Delta t$ . . . . .	39

# List of Tables

3.1	Physical parameters used in the nonlinear model . . . . .	13
-----	---	----

# Chapter 1

## Introduction

### 1.1 What are Numerical Models?

Numerical models are widely used in Meteorology. These numerical models are effectively a computer program that takes current weather data and then solves equations to produce a prediction of the future conditions. In 1950 a team of researchers led by the American meteorologist Jule Charney managed to produce the first computer-generated weather forecast [2]. The forecast was a major step forward and eventually developed into an area called numerical weather prediction (NWP). This development transformed meteorology from a collection of rules of thumb into a rigorous quantitative science. NWP models are trying to solve a number of mathematical equations that are nonlinear. Being nonlinear they are impossible to solve exactly but the model can use a numerical method to give an approximate solution. Models are started using initial data that we have taken from satellites, radiosonde ascents or weather stations. The initial data is put into the model and run to give some output data representing the future state of the atmosphere.

### 1.2 Sources of Error

The output data from the model is only an approximation and therefore contains some form of error compared to what the atmosphere will actually do. For example, the initial data used to initialise the model will contain measurement errors, which propagate through the model and become output errors. There are also some areas

of the globe where observations cannot easily be made. Therefore it depends on the area of the atmosphere you are modelling in order to get accurate initial data. However, data assimilation techniques combine previous forecasts with the incomplete observations to provide a more complete and more accurate set of initial data. It is still difficult to predict the exact state of the atmosphere at any given time and as a result the uncertainty in the initial data is not negligible.

There is also uncertainty in the lateral boundary conditions in non-global models. The size and shape of the domain that is being modelled has to be considered, because the state of the atmosphere has to be specified along the boundaries in order to allow the model to run. Often these boundary conditions will be obtained from a lower-resolution model with a wider domain, but they will inevitably contain errors.

Finally, spatial and time stepping errors are present in the model. The partial differential equations within all numerical models are approximated by a variety of numerical schemes. In reality time and space differencing are often considered separately as both provide different problems. When a model performs a numerical integration, the solution is known at each grid point on the spatial mesh. As a result, it is relatively simple in principle to have high-order approximations to spatial derivatives, involving more than just the nearest neighbours. However, with time derivatives, storage limitations are a problem and usually the only time levels available are from the previous iteration [2]. The idea is to have a spatial mesh where  $\Delta x$  and  $\Delta y$  (and  $\Delta z$  or  $\Delta p$ ) are as small as possible in order to get the most accurate solution. Similarly, the time step  $\Delta t$  needs to be as small as possible.

It has previously been shown that reducing the simulation errors of prognostic variables such as zonal wind and temperature, allows better simulations for diagnostic variables such as precipitation [9]. Figure 1.1 shows the zonal-mean zonal wind error and temperature error for the leapfrog scheme and second-order Adams-Bashforth respectively. The errors being considerably smaller for the second-order Adams-Bashforth method. Hence this outlines the importance of reducing time step errors in NWP models. The results of different time-stepping schemes in general circulation models give evidence that climate simulations are sensitive not only to physical parametrisations of subgrid-scale processes but also to the numerical method employed [5].

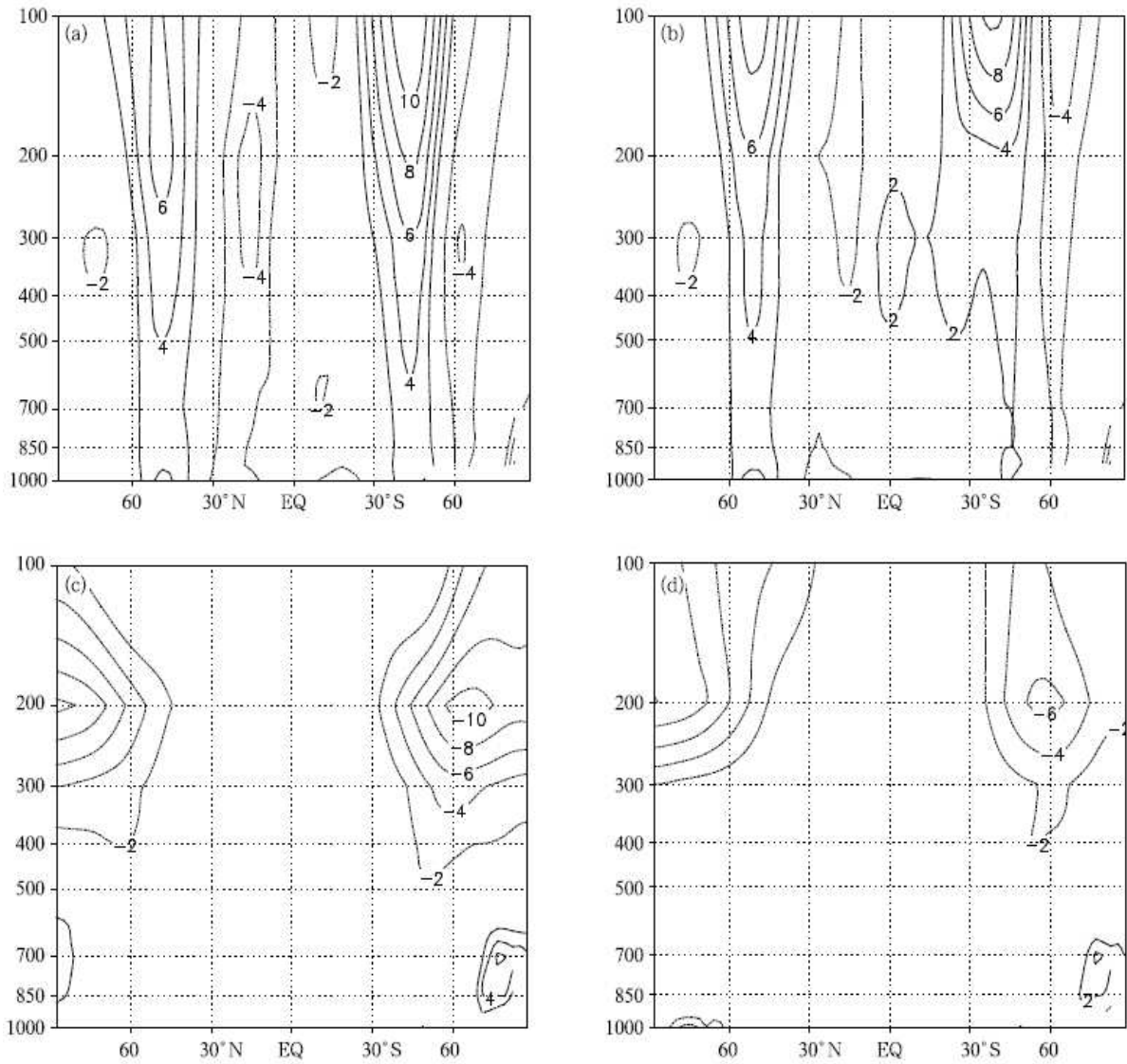


**Figure 1.1:** Comparison between the (a) zonal-mean zonal wind error (m/s) using the leapfrog scheme, (b) zonal-mean zonal wind error (m/s) using the second-order Adams-Bashforth scheme, (c) temperature error using the leapfrog scheme and (d) temperature error using the second-order Adams-Bashforth method. Taken from [9].

## 1.3 Aims

In this dissertation we will only consider time-differencing schemes and will not consider different space-differencing schemes. This is done to isolate the time-stepping errors. The aims are:

- To implement a number of time-differencing schemes in a simple nonlinear grid-point numerical model and compare the time step errors in the schemes.
- To compare the results with the predictions of simple linear analyses and numerical ocean models.
- To decide whether the schemes could and should be implemented into existing NWP models.

## 1.4 Outline

We begin the dissertation by considering time-differencing schemes [3] while reviewing previous work on the Robert-Asselin filter and a recently proposed modification to it [6]. The different time step methods include the leapfrog scheme with a Robert-Asselin filter and modified family of filters. Also the Adams-Bashforth family of schemes will be considered [5]. In Chapter 3 we will discuss the nonlinear numerical model that will be used to test each of the schemes explained in Chapter 2. Chapter 4 will show the numerical results from the model and provide an analysis of the schemes. Chapter 5 will test the sensitivity of the nonlinear model. Finally, Chapter 6 will conclude the dissertation by summarising the previous chapters and suggesting further work.

# Chapter 2

## Time-Differencing Schemes

In this Chapter we discuss various time-differencing schemes. We first consider the Robert-Asselin filter and apply it to the leapfrog scheme. We then consider the first, second and third order Adams-Bashforth schemes.

### 2.1 Leapfrog Scheme

The leapfrog scheme can be expressed using the formula

$$x_{n+1} = x_{n-1} + 2\Delta t F(x_n) \tag{2.1}$$

where  $x_{n+1}$  is the approximate solution to be determined given the other variables.

The leapfrog scheme uses information at three different time levels  $t_{n-1}$ ,  $t_n$  and  $t_{n+1}$  with a total difference of  $2\Delta t$ . The numerical approximation to the derivative is known as a centered difference scheme. One problem with this scheme is the  $t_{n-1}$  time level as we only know our initial variable at time  $t_n$  and not also  $t_{n-1}$ . This is overcome by using a simple forward step first. Then it is possible to carry out the integration using the leapfrog scheme. The leapfrog scheme yields second-order accuracy.

However, problems tend to arise with the leapfrog scheme as it generates a computational mode. The most serious problem is the time splitting instability that develops when used to model nonlinear fluid dynamics [3]. The computational mode is created by the numerical scheme and is different from the actual solution

that we are after. The actual solution is known as the physical mode. Depending on the problem being solved the computational mode can cause the numerical solution to grow exponentially. The rate at which this occurs depends on the time step  $\Delta t$ . Towards the end of the numerical integration the numerical solution deviates further away from the actual solution. The reason for this is the integration goes from the  $t_{n-1}$  time point to the  $t_{n+1}$  time point and misses out at even and odd time steps the  $t_n$  time point. By missing out the  $t_n$  time point this causes the numerical solution to drift apart as you step forward through the integration and as result generates the so-called computational mode. The simple leapfrog scheme is unstable but can be stabilised using the Robert-Asselin filter.

### 2.1.1 Leapfrog Scheme with Robert-Asselin Filter

The Robert-Asselin filter was designed specifically for the leapfrog scheme in 1966 by Robert and in 1972 Asselin showed that it dampens the computational mode but leaves the physical mode relatively undamped [1][6][7]. Since then it has become known as the Robert-Asselin filter. After each leapfrog step, the filter mixes solutions from three consecutive time points at  $t_{n-1}$ ,  $t_n$  and  $t_{n+1}$  which can be seen from Figure 2.1. The solution at the inner point at time  $t_n$  is displaced by

$$d = \frac{\nu}{2} [x_{n-1} - 2x_n + x_{n+1}] \quad (2.2)$$

where  $\nu$  is the filter parameter and the values  $x_{n-1}$ ,  $x_n$  and  $x_{n+1}$  correspond to the time points  $t_{n-1}$ ,  $t_n$  and  $t_{n+1}$  respectively. Typically the filter parameter is taken to be 0.01. In Chapter 4 we will see the importance of the filter parameter  $\nu$ .

The leapfrog scheme with the Robert-Asselin filter suffers from numerical problems. The filter weakly suppresses the physical mode. Physical quantities are not necessarily conserved by the discretised equations in the model when the filter is switched on. The Robert-Asselin filter degrades the numerical accuracy of the leapfrog scheme from second order to first order. The degrading of the scheme limits the range of time steps that can be implemented without the loss of accuracy. This is why higher order schemes are often preferred but usually cost more to implement.

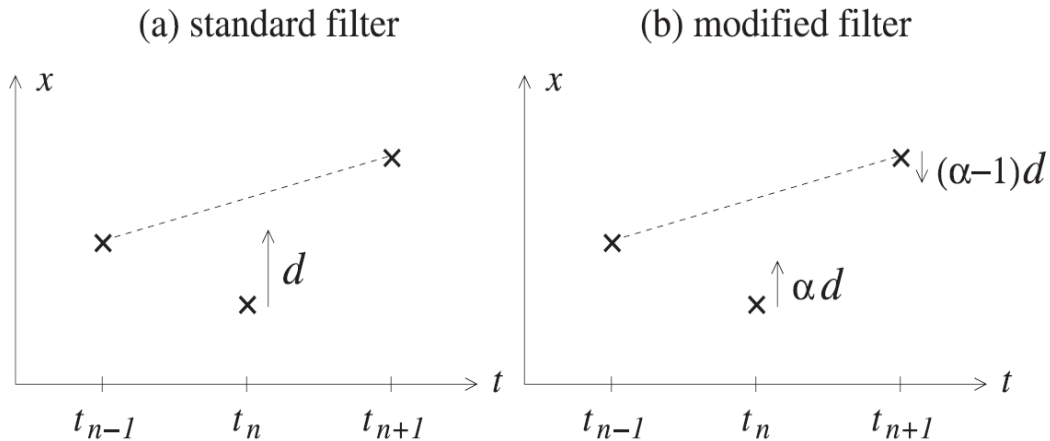


**Figure 2.1:** Comparison between the (a) the standard Robert-Asselin filter and (b) proposed modified filters. Taken from [7].

### 2.1.2 Leapfrog with Modified Filter

Due to the wide usage of the Robert-Asselin filter we will look at a recent modification that was proposed to the Robert-Asselin filter [6]. Figure 2.1 shows that with the modified filter the inner point and right outer point are displaced by  $\alpha d$  and  $(\alpha - 1)d$  respectively where  $\alpha$  is between 0 and 1. If the coefficient  $\alpha$  was taken to be 1 then we would have the standard filter explained previously. If  $\alpha = 0$  then the modification would only displace the right outer point. However, if  $\alpha = 0.5$  then the inner and right outer points would be displaced equally and oppositely, conserving the three-time-level mean state and preserving the second-order accuracy of the leapfrog scheme. We will consider these cases of  $\alpha = 1$ ,  $\alpha = 0.5$  and  $\alpha = 0$  in Chapter 4.

## 2.2 Adams-Bashforth Schemes

Furthermore we will consider the Adams-Bashforth family of schemes. These are relatively simple linear multistep methods that can be used as a replacement to the leapfrog scheme. We will discuss the first, second and third order schemes.

### 2.2.1 First-Order

The first-order Adams-Bashforth method is simply a forward difference scheme and can be expressed using the formula

$$x_{n+1} = x_n + \Delta t F(x_n) \quad (2.3)$$

We use this forward scheme for the first iteration when using the leapfrog scheme. We would rather consider Adams-Bashforth second or third-order with increased numerical accuracy than just the first order method as they would not cost much more to implement.

### 2.2.2 Second-Order

The second-order Adams-Bashforth scheme can be expressed using the formula

$$x_{n+1} = x_n + \frac{\Delta t}{2} [3F(x_n) - F(x_{n-1})] \quad (2.4)$$

Here we are considering points at two previous time levels which is similar to the leapfrog scheme but is not subject to time splitting. The two previous time levels being  $x_n$  and  $x_{n-1}$ . Therefore the Robert-Asselin filter is not required. The disadvantage of the second order Adams-Bashforth method is when it is used to model oscillatory behaviour the physical mode is subject to instability as the waves tend to amplify. This can be controlled somewhat if the time steps are small over a small integration [3], but the scheme is not used in practice for this reason.

### 2.2.3 Third-Order

The third-order Adams-Bashforth scheme can be expressed using the formula

$$x_{n+1} = x_n + \frac{\Delta t}{12} [23F(x_n) - 16F(x_{n-1}) + 5F(x_{n-2})] \quad (2.5)$$

Although the scheme is more accurate, we need to consider points at three previous time levels to determine  $x_{n+1}$ . The three previous time levels being  $x_n$ ,  $x_{n-1}$  and

$x_{n-2}$ . The third-order Adams-Bashforth method is an explicit scheme that requires one function evaluation per time step. The only potential problem is the storage requirements that prove to be a problem with all higher order schemes. Using the third-order Adams-Bashforth method eliminates the computational mode without introducing any other parameters [3].

# Chapter 3

## Model Description

In this Chapter we will discuss the QUAGMIRE v1.3 model that will be used to test the behaviour of the time-differencing schemes outlined in Chapter 2. We will look at the model equations along with the assumptions that have been made. Also, we will look at initialising the model to gather suitable initial conditions.

### 3.1 QUAGMIRE v1.3

QUAGMIRE v1.3 is a quasi-geostrophic model that performs high-resolution simulations for investigating rotating fluid flows [8]. This is the fourth version of the model with many adaptations being made to the source code and diagnostic software to make QUAGMIRE v1.3 more efficient. The model was originally designed for simulating two-layer laboratory experiments in a rotating annulus. The fluid flow in this system is dynamically similar to, for example, the mid-latitude jet streams in the atmosphere and the Antarctic Circumpolar Current (ACC) in the ocean. The jet streams being the fast flowing cylindrical flows of air in the upper atmosphere and the ACC being an important oceanic moving current. Dynamical similarity makes it possible to scale results from laboratory experiments to predict corresponding results for the full scale system. This statement is true despite the fact that typical length and time scales may differ by several orders of magnitude.

Figure 3.1 shows the two layers in the model with a constant jet stream speed in the upper layer (layer 1) and a constant weaker jet stream speed in the lower layer (layer 2). It is this interface between the two layers upon which perturbations

may grow due to baroclinic instability. Baroclinic instability being an important mechanism that influences mid-latitude synoptic scale patterns that cause initial disturbances. These disturbances or perturbations are wave-like features that grow and decay with time.

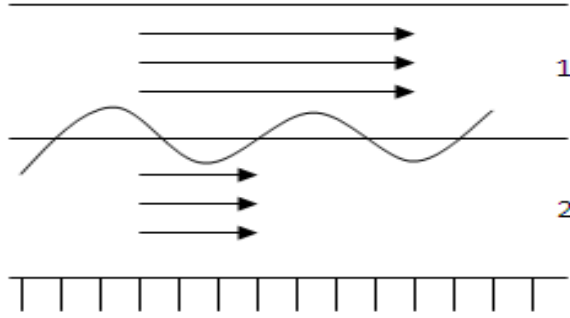


**Figure 3.1:** *Two layer diagram showing the interface between the two layers where waves will amplify and decay in the QUAGMIRE v1.3 model.*

## 3.2 Equations

The model equations are solved in each of the two layers shown in Figure 3.1. Equation 3.1 corresponds to the upper layer and equation 3.3 is solved in the lower layer. Equation 3.1 is the potential vorticity change with time which is equal to an advection term plus viscous Ekman damping and wind stress forcing at the upper boundary. Equation 3.3 is similar but has no wind stress forcing. It is these equations that are solved numerically in the model. Each parameter is defined in Table 3.1.

$$\frac{\partial q_1}{\partial t} = \frac{1}{r} \frac{\partial \psi_1}{\partial \theta} \frac{\partial q_1}{\partial r} - \frac{1}{r} \frac{\partial \psi_1}{\partial r} \frac{\partial q_1}{\partial \theta} - \frac{\sqrt{\Omega \nu_1}}{H} [\nabla^2 \psi_1 + \chi_2 \nabla^2 (\psi_1 - \psi_2)] + \frac{2\Delta\Omega\sqrt{\Omega\nu_1}}{H} \quad (3.1)$$

where

$$q_1 = \nabla^2 \psi_1 + \frac{f^2}{g'H} (\psi_2 - \psi_1) + \frac{f}{H} \frac{r^2 \Omega^2}{2g} \quad (3.2)$$

$$\frac{\partial q_2}{\partial t} = \frac{1}{r} \frac{\partial \psi_2}{\partial \theta} \frac{\partial q_2}{\partial r} - \frac{1}{r} \frac{\partial \psi_2}{\partial r} \frac{\partial q_2}{\partial \theta} - \frac{\sqrt{\Omega \nu_2}}{H} [\nabla^2 \psi_2 + \chi_1 \nabla^2 (\psi_2 - \psi_1)] \quad (3.3)$$

where

$$q_2 = \nabla^2 \psi_2 - \frac{f^2}{g'H} (\psi_2 - \psi_1) - \frac{f}{H} \frac{r^2 \Omega^2}{2g} \quad (3.4)$$

From equation 3.1-3.4 the terms have been separated out to show the physical response to each where  $i = 1$  for the upper layer or  $i = 2$  for the lower layer. We can now see which terms are responsible for the advection, forcing and dissipation.

$$\frac{1}{r} \frac{\partial \psi_i}{\partial \theta} \frac{\partial q_i}{\partial r} - \frac{1}{r} \frac{\partial \psi_i}{\partial r} \frac{\partial q_i}{\partial \theta} = \text{Advection} \quad (3.5)$$

$$\frac{\sqrt{\Omega \nu_1}}{H} [\nabla^2 \psi_i + \chi_i \nabla^2 (\psi_i - \psi_i)] = \text{Viscous Ekman damping} \quad (3.6)$$

$$\frac{2\Delta\Omega\sqrt{\Omega\nu_1}}{H} = \text{Wind stress forcing} \quad (3.7)$$

The potential vorticity  $q$  is the sum of the relative vorticity, vortex stretching/compression and the  $\beta$ -effect.

$$\nabla^2 \psi_2 = \text{Relative vorticity} \quad (3.8)$$

$$\frac{f^2}{g'H} (\psi_2 - \psi_1) = \text{Vortex stretching/compression} \quad (3.9)$$

$$\frac{f}{H} \frac{r^2 \Omega^2}{2g} = \beta - \text{effect} \quad (3.10)$$

Parameter	Meaning
$\psi_1$	Stream function in the upper layer (layer 1)
$\psi_2$	Stream function in the lower layer (layer 2)
$q_1$	Potential vorticity in the upper layer (layer 1)
$q_2$	Potential vorticity in the lower layer (layer 2)
$\Omega$	Angular velocity
$f$	Coriolis parameter (usually $10^{-4}$ ) for mid-latitudes)
$H$	Scale height
$g$	Acceleration due to gravity
$g'$	Reduced gravity
$\nu_1$	Kinematic viscosity in the upper layer (layer 1)
$\nu_2$	Kinematic viscosity in the lower layer (layer 2)
$r$	Polar coordinate
$\theta$	Polar coordinate
$z$	Polar coordinate
$\chi_1$	Perturbation potential vorticity in the upper layer (layer 1)
$\chi_2$	Perturbation potential vorticity in the lower layer (layer 2)
$\nabla$	Laplacian operator

**Table 3.1:** *Physical parameters used in the nonlinear model*

The horizontal grid points are shown in Figure 3.2. For the mid-latitudes, normally  $30^\circ - 60^\circ\text{N}$  if the Northern hemisphere atmospheric jet stream is being represented or  $30^\circ - 60^\circ\text{S}$  if the oceanic Antarctic Circumpolar Current is being represented.

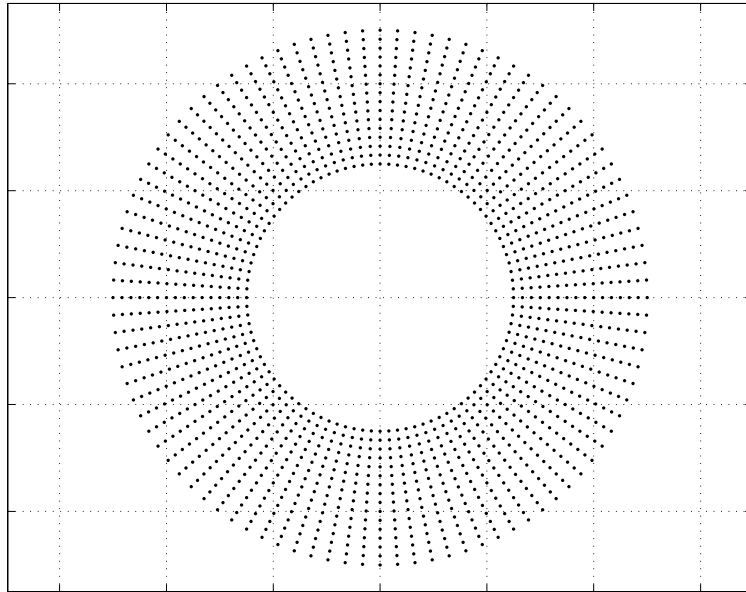


**Figure 3.2:** Shows the grid points across mid-latitudes, where the model fluid flows are solved. There are 16 grid points in the latitudinal direction and 96 in the longitudinal direction equating to grid points every  $4^\circ$  of latitude and  $2^\circ$  of longitude.

### 3.3 Assumptions

In order to derive the above equations, assumptions about the model have to be made and may affect the results. The main assumptions [8] were:

- Incompressible fluids.
- Inviscid fluid interiors meaning a Reynolds number  $\gg 1$ .
- Vertical fluid interior columns.
- Linear Ekman pumping and suction.

- Atmosphere in hydrostatic balance.
- Ekman layer depths  $\ll$  scale height  $H$ .
- Rossby number  $\ll 1$ .
- Reduced gravity  $g' \ll g$

The first initial assumption is to assume incompressible fluids. This means when you move a fluid parcel the density is conserved. It is often represented by the equation

$$\nabla \cdot u = 0 \tag{3.11}$$

where  $u$  is the fluid velocity.

The Reynolds number ( $Re$ ) and Rossby number ( $Ro$ ) are non-dimensional numbers that are used to distinguish the behaviour of fluid flows. Both these assumptions are good approximations for the large-scale flow in the atmosphere and ocean. The Reynolds number is a ratio between the inertial and viscous forces. The Reynolds number is expressed using the formula

$$Re = \frac{UL}{\nu} \tag{3.12}$$

where  $U$  is the fluid velocity,  $L$  is a length scale and  $\nu$  is the viscosity. Here we are assuming a Reynolds number  $\gg 1$  which means the inertial forces are much larger than the viscous forces acting on the fluid parcel [4]. The Rossby number is the ratio of inertial to Coriolis forces acting on the fluid flow. The Rossby number is given by

$$Ro = \frac{U}{fL} \tag{3.13}$$

where  $U$  is the fluid velocity,  $L$  is a length scale and  $f$  is the Coriolis parameter. We are assuming that the Coriolis force acting is much larger than inertial forces [4].

### 3.4 Initialisation

The model uses a leapfrog time-stepping scheme with a Robert-Asselin filter. We may refer to this as the default time-stepping scheme. The Robert-Asselin filter  $\nu$  is taken to be 0.01 and a time step  $\Delta t = 0.0008$  is used (in suitable units which are not of interest here). The model was run initially until the amplitude of the baroclinic waves began to stabilise. Figure 3.3 initially shows a large increase in amplitude due to the baroclinic instability, but gradually decays through time. At the end of the run visually the amplitude looks fairly constant but there are oscillations of a smaller amplitude which cannot be seen here.

This spin-up run provided an initial state and time to begin the different time stepping schemes. This way it would be possible to compare the schemes more carefully. The state at time 800 will be used as the initial condition for the experiments in the next Chapter. Note that, since we are interested only in amplitude changes when new time-stepping schemes are used, the units of the absolute amplitudes will be considered to be arbitrary.

Figure 3.4 shows the initial state of streamfunction perturbations at time 800. The red areas represent positive perturbations and the blue areas negative perturbations. The red regions being cyclonic motion and blue regions being anticyclonic motion. The behaviour of the streamfunction field is similar to the movement of pressure patterns at the surface. If this was allowed to run further through time these features would develop further causing wave troughs and crests around the globe due to baroclinic instability.

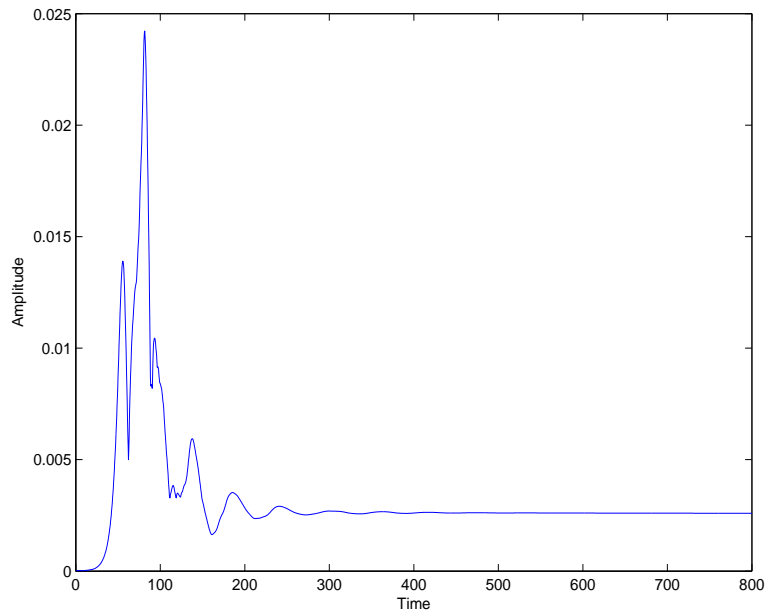


**Figure 3.3:** Shows the amplitude of the perturbation between the two layers in the model for  $\Delta t = 0.0008$  using a leapfrog scheme with Robert-Asselin filter of 0.01.

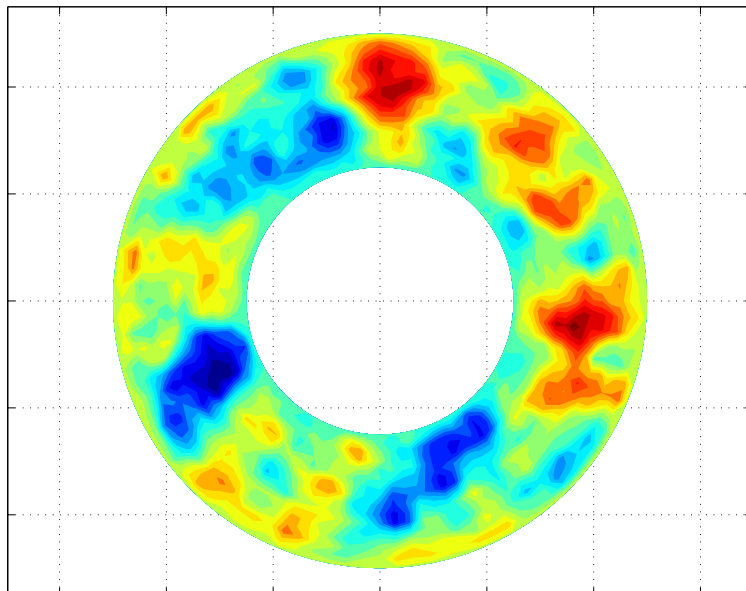


**Figure 3.4:** Shows the perturbations in streamfunction for the upper layer at time 800.

# Chapter 4

## Numerical Results

In this Chapter we will compare the results from the time-differencing schemes that we have implemented in the QUAGMIRE v1.3 model. We will look at the associated amplitude errors with the schemes.

### 4.1 Leapfrog with Robert-Asselin Filter

We will first begin with the default time-stepping scheme in the model by varying the filter parameter  $\nu$ . By only changing  $\nu$  it helps to determine the affect the filter parameter has on the results. We will consider the standard filter and modified filters in turn.

#### 4.1.1 Standard Filter $\alpha = 1$

Firstly, the standard Robert-Asselin filter was used with  $\alpha = 1$ . The default filter parameter  $\nu$  is 0.01 and this is a typical value that is used in numerical models. Figure 4.1 shows the amplitude of the potential vorticity between the two layers in the model for filter parameters ranging from 0.005 to 1.0. A filter parameter of 1.0 would not be used in reality but is shown for the purpose of the experiment. As  $\nu$  increases a large amount of ringing becomes apparent at the the start of the time integration. Ringing is a general phenomenon associated with the time domain oscillation. The magnitude of the oscillations are of order  $10^{-3}$  which shows the differences in amplitude are fairly small. Further through the integration the ringing

becomes less apparent and the amplitude becomes smoother. As  $\nu$  increases the final amplitude becomes larger. Figure 4.2 shows the amplitude relative to the base amplitude. This shows the differences in amplitude becoming larger as  $\nu$  increases. Figure 4.3 shows the final amplitude versus  $\nu$ . As  $\nu$  increases the final amplitude increases at a faster rate. The magnitude of the amplitude error [2][3] associated with the scheme is given by

$$|A| = 1 - \frac{\nu}{2(1 - \nu)}\omega^2\Delta t^2 \quad (4.1)$$

where  $\nu$  is the filter parameter,  $\Delta t$  is the time step and  $\omega$  is the angular frequency.

According to the amplitude error as  $\nu$  gets larger the final amplitude should become smaller if  $\omega\Delta t$  is held fixed. Therefore the linear theory is not valid as the wave amplitude is growing which can be seen on Figure 4.3.

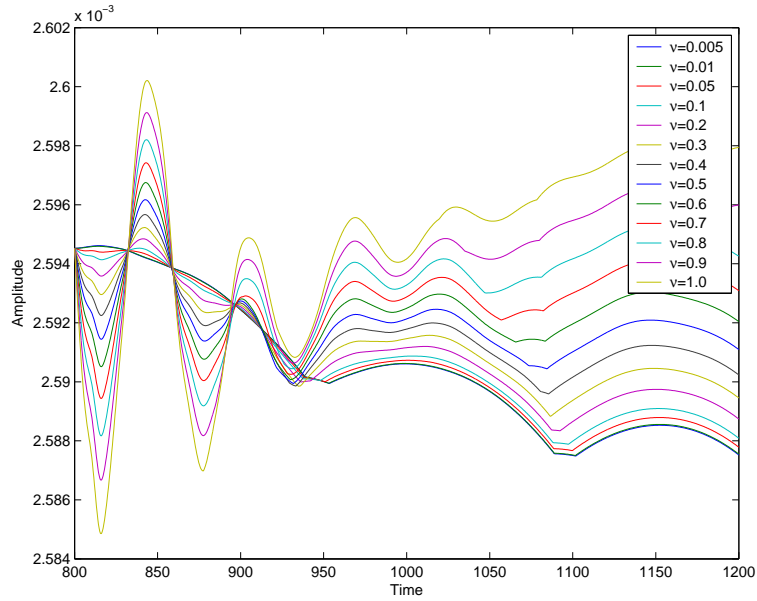


**Figure 4.1:** Leapfrog scheme with standard Robert-Asselin filter for a range of different filter parameters. Shows the amplitude of the perturbation between the two layers in the model for  $\alpha = 1$ .

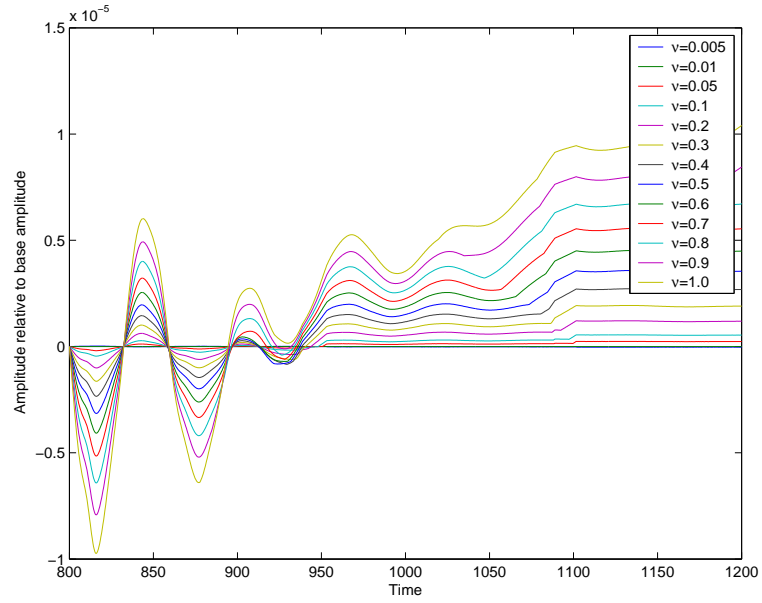


**Figure 4.2:** Leapfrog scheme with standard Robert-Asselin filter for a range of different filter parameters. Shows the amplitude of the perturbation between the two layers relative to the base amplitude for  $\alpha = 1$ . The base amplitude being for the filter parameter  $\nu = 0.01$ .

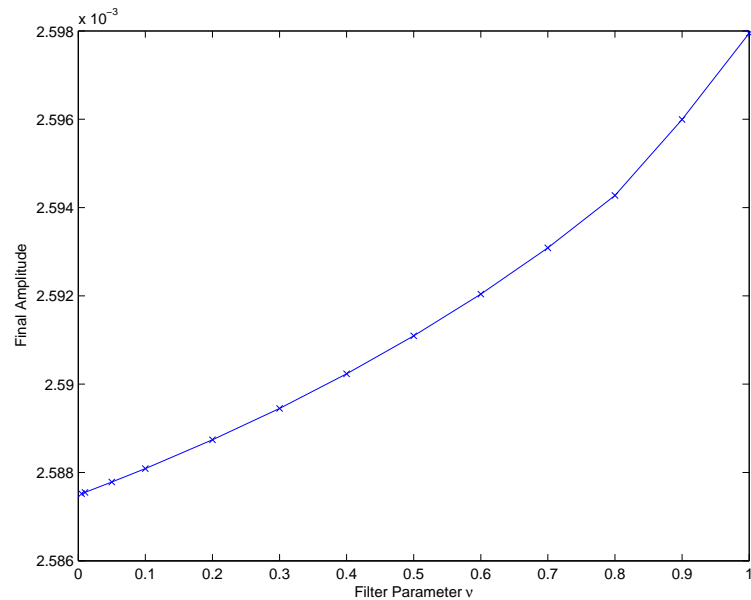


**Figure 4.3:** Leapfrog scheme with standard Robert-Asselin filter for a range of different filter parameters with  $\alpha = 1$ . Shows the final amplitude versus the filter parameter  $\nu$ .

### 4.1.2 Modified Filter $\alpha = 0.5$

We shall now consider the modified filter with  $\alpha = 0.5$ . There is clearly a significant difference between the modified filter and standard filter as shown in Figure 4.4. The order of accuracy has increased from first-order to third-order [7]. The amplitude is less influenced by  $\nu$ . The ringing has become suppressed at the beginning of the integration. However, there is ringing which can be seen on Figure 4.5. As we are using the default time step which was the same for initialising the model then the ringing is less obvious. It is more clear when we change the time step. Figure 4.5 also shows the noise created by the irregular wave pattern between each time step which cannot be seen with the standard filter. This is because we are displacing the inner and outer points rather than just the inner point. Figure 4.6 and 4.3 are similar as the final amplitude increases with  $\nu$ . However, the linear theory suggests that the amplitude should decrease as with the standard filter.

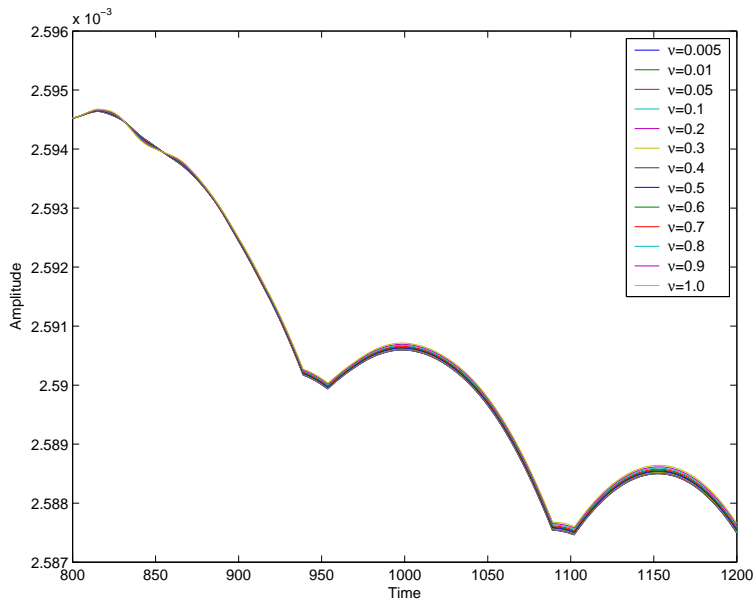


**Figure 4.4:** *Leapfrog scheme with modified Robert-Asselin filter for a range of different filter parameters. Shows the amplitude of the perturbation between the two layers in the model for  $\alpha = 0.5$ .*

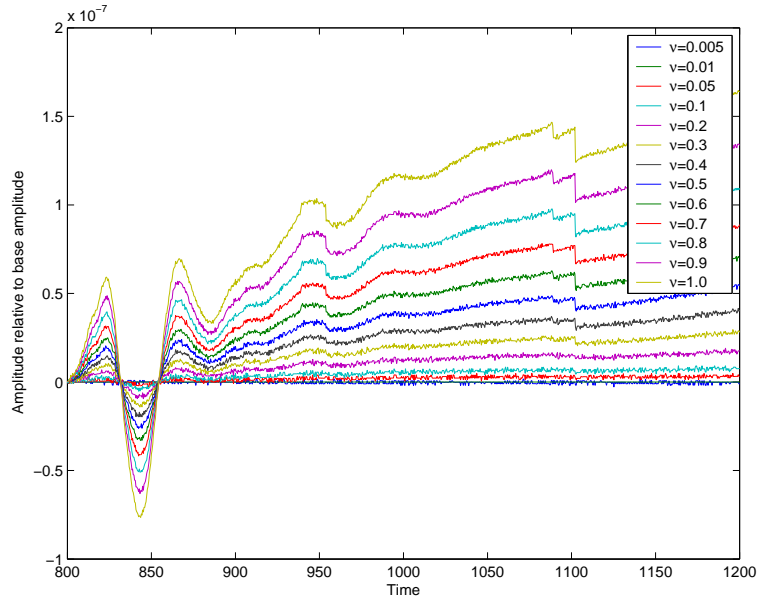


**Figure 4.5:** Leapfrog scheme with standard Robert-Asselin filter for a range of different filter parameters. Shows the amplitude of the perturbation between the two layers relative to the base amplitude for  $\alpha = 0.5$ . The base amplitude being for the filter parameter  $\nu = 0.01$ .

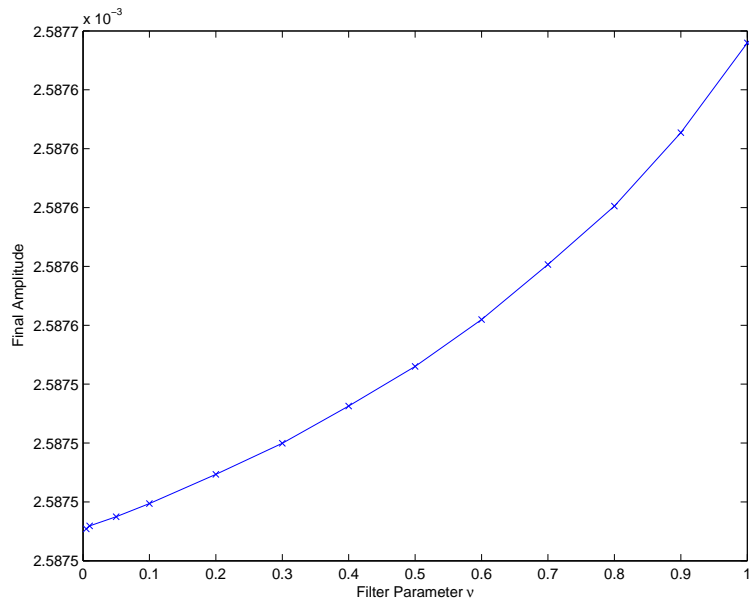


**Figure 4.6:** Leapfrog scheme with standard Robert-Asselin filter for a range of different filter parameters with  $\alpha = 0.5$ . Shows the final amplitude versus the filter parameter  $\nu$ .

### 4.1.3 Modified Filter $\alpha = 0$

Finally, the modified filter with  $\alpha = 0$  only displaces the outer point. This scheme is unconditionally unstable. Once  $\nu > 0.7$  the model becomes unstable and terminates. This scheme is equal and opposite to the standard filter when  $\alpha = 1$ . The amplitude at the end of the integration decreases as  $\nu$  increases. This can be seen from Figure 4.7 and 4.8. The ringing is apparent at the start of the time integration for the larger  $\nu$ . Figure 4.9 shows the final amplitude decreasing as  $\nu$  increases which does agree with the linear theory because equation 4.1 gives an amplitude error less than 1.

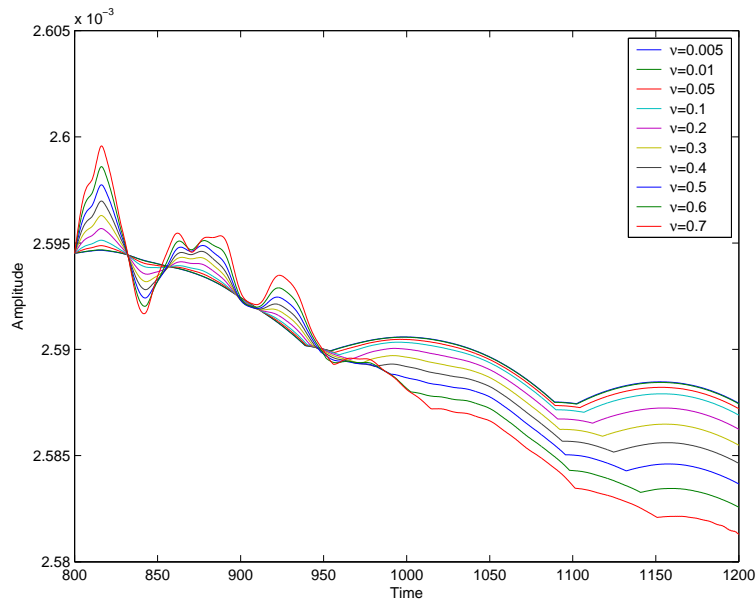


**Figure 4.7:** Leapfrog scheme with modified Robert-Asselin filter for a range of different filter parameters. Shows the amplitude of the perturbation between the two layers in the model for  $\alpha = 0$ .

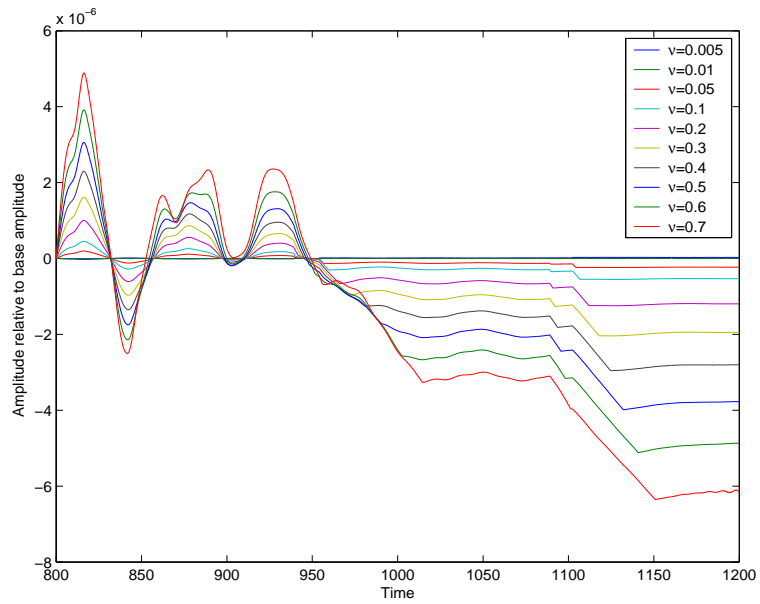


**Figure 4.8:** Leapfrog scheme with standard Robert-Asselin filter for a range of different filter parameters. Shows the amplitude of the perturbation between the two layers relative to the base amplitude for  $\alpha = 0$ . The base amplitude being for the filter parameter  $\nu = 0.01$ .

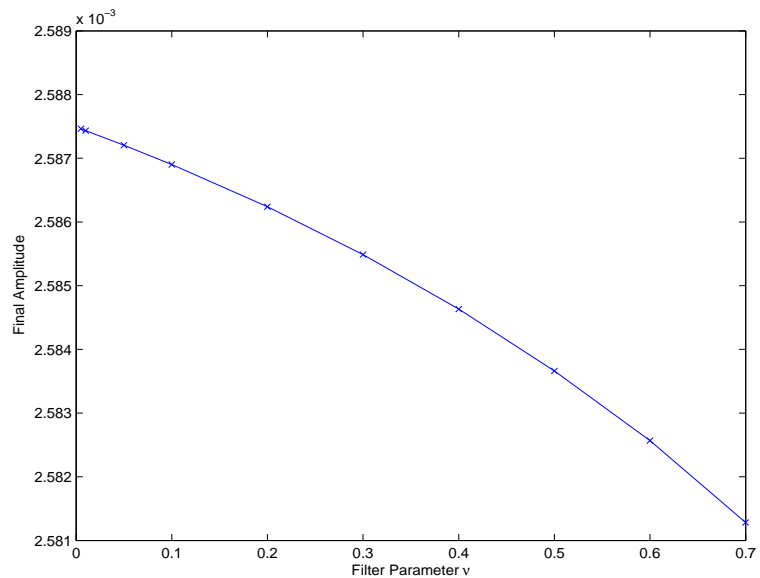


**Figure 4.9:** Leapfrog scheme with standard Robert-Asselin filter for a range of different filter parameters with  $\alpha = 0$ . Shows the final amplitude versus the filter parameter  $\nu$ .

## 4.2 Adams-Bashforth Schemes

We shall now consider the Adams-Bashforth schemes which we will run from the initial conditions set by the default scheme.

### 4.2.1 First-Order

The first-order Adams-Bashforth scheme becomes unstable before the end of the time integration as you can see from Figure 4.10. The exponential growth in wave amplitude causes the model to stop the numerical integration. The amplitude error [3] is given by

$$|A| = 1 + \frac{\omega^2 \Delta t^2}{2} \quad (4.2)$$

where  $\Delta t$  is the time step and  $\omega$  is the angular frequency. As  $|A| > 1$  the scheme is amplifying. The initial amplitude are small but grow in amplitude extremely fast.

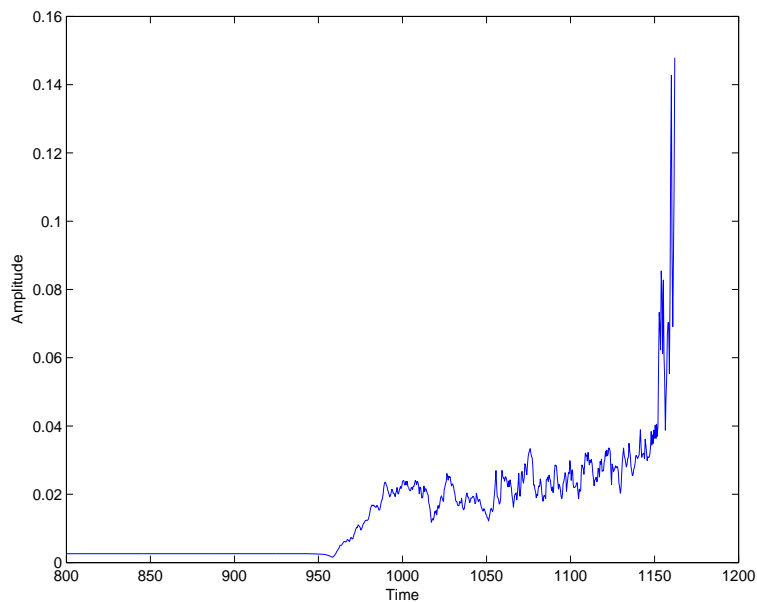


**Figure 4.10:** *First-order Adams-Bashforth scheme. Shows the amplitude of the perturbation between the two layers in the model.*

## 4.2.2 Second-Order

We know the first-order Adams-Bashforth method is unstable so we shall now use the second-order method. Using the default time step  $\Delta t = 0.0008$  the scheme is stable over the whole integration. Figure 4.11 shows as the time step increases the final amplitude also increases. The amplitude increases more rapidly for larger  $\Delta t$ . This is correct with the linear theory as the associated amplitude error suggests an increase in amplitude [3]. This is given by

$$|A| = 1 + \frac{\omega^4 \Delta t^4}{4} \quad (4.3)$$

where  $\Delta t$  is the time step and  $\omega$  is the angular frequency. We will derive the amplitude error in Section 4.3.

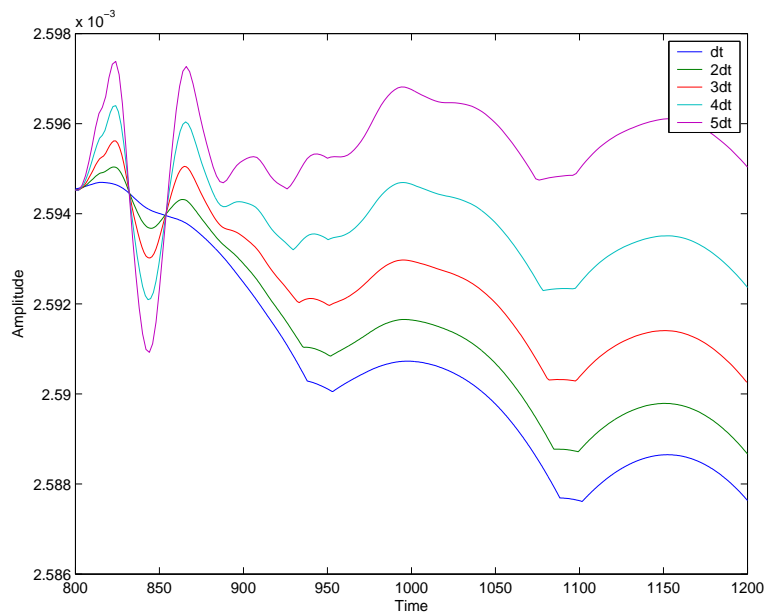


**Figure 4.11:** *Second-order Adams-Bashforth scheme. Shows the amplitude of the perturbation between the two layers in the model for increasing  $\Delta t$ .*

### 4.2.3 Third-Order

The third-order Adams-Bashforth is more accurate again. As  $\Delta t$  increases the difference in amplitude is smaller than the second-order Adams-Bashforth method. However, this is what we expect. According to the linear theory the final amplitude should decrease for larger  $\Delta t$  but the amplitude has increased as Figure 4.12 shows. This could be due to the length of the integration. If we extended the this further the amplitude may decrease. It could be also be due to the derivation of the amplitude error as these are derived from Taylor series expansions. The amplitude error [3] is given by

$$|A| = 1 - \frac{3\omega^4 \Delta t^4}{4} \quad (4.4)$$

where  $\Delta t$  is the time step and  $\omega$  is the angular frequency. Due to the third-order accuracy, the oscillations caused by ringing are not as large as the second-order method.

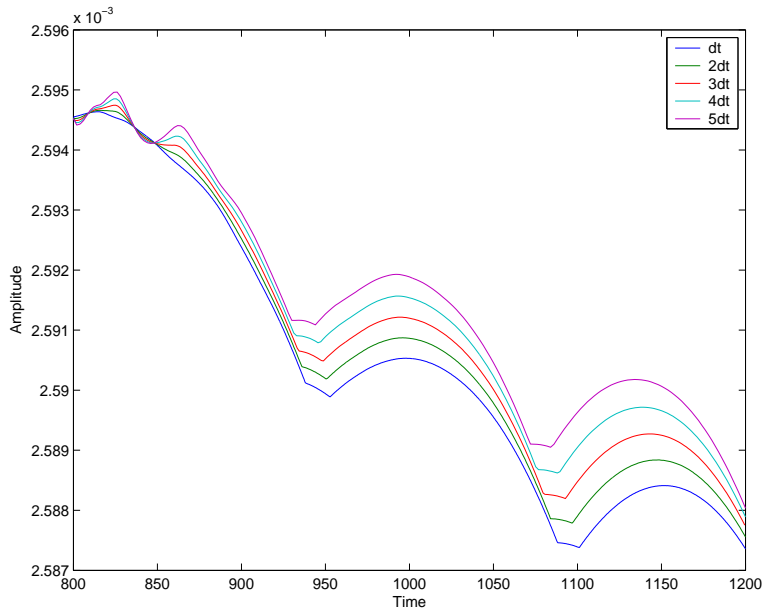


**Figure 4.12:** *Third-order Adams-Bashforth scheme. Shows the amplitude of the perturbation between the two layers in the model for increasing  $\Delta t$ .*

### 4.3 Deriving Amplitude Errors

The amplitude errors tell you about the behaviour of the scheme. Here we will derive the amplitude error for the second-order Adams-Bashforth method. Let us consider the oscillation differential equation for the complex variable  $F(t)$  such that

$$\frac{dF}{dt} = i\omega F \quad (4.5)$$

where  $i = \sqrt{-1}$  and  $\omega$  is the angular frequency.

Equation 2.4 can be written in terms of  $F$  to give

$$F^{n+1} = F^n + \frac{\Delta t}{2} [3i\omega F^n - i\omega F^{n-1}] \quad (4.6)$$

We shall now define an amplification factor  $A$  where

$$A = \frac{F^{n+1}}{F^n} = \frac{F^n}{F^{n-1}} \quad (4.7)$$

Now using equation 4.7 we can rewrite equation 4.6 in terms of  $F^n$  to give

$$AF^n = F^n + \frac{\Delta t}{2} \left[ 3i\omega F^n - \frac{i\omega F^n}{A} \right] \quad (4.8)$$

Then we can multiply by  $A$  to give a quadratic equation in terms of  $A$ , therefore

$$A^2 - A \left[ \frac{3}{2}i\omega\Delta t + 1 \right] + \frac{i\omega\Delta t}{2} = 0 \quad (4.9)$$

If we let  $x = i\omega\Delta t$  then equation 4.9 becomes

$$A^2 - A \left[ \frac{3}{2}x + 1 \right] + \frac{x}{2} = 0 \quad (4.10)$$

which makes it easier to solve.

Using the quadratic formula we get

$$A_{\pm} = \frac{\frac{3}{2} + 1 \pm \sqrt{(\frac{3}{2}x + 1)^2 - 4(1)(\frac{x}{2})}}{2(1)} \quad (4.11)$$

and the square root can be expanded using a Taylor series expansion to give

$$A_{\pm} = \frac{\frac{3}{2}x + 1 \pm 1 - \frac{x}{2} + x^2 - \frac{x^3}{2} - \frac{x^4}{4} + \dots}{2} \quad (4.12)$$

The amplitude error  $A_+$  is for the physical mode and  $A_-$  is the amplitude error for the computational mode. The physical mode being the approximate to the original differential equation.

If we now substitute  $x = i\omega\Delta t$  back into equation 4.12 we get

$$A_+ = 1 + i\omega\Delta t - \frac{\omega^2\Delta t^2}{2} + \frac{i\omega^3\Delta t^3}{4} - \frac{\omega^4\Delta t^4}{8} + \dots \quad (4.13)$$

$$A_- = \frac{i\omega\Delta t}{2} + \omega^2\Delta t^2 - \frac{i\omega^3\Delta t^3}{2} + \frac{\omega^4\Delta t^4}{4} + \dots \quad (4.14)$$

We can determine the magnitudes  $|A_+|$  and  $|A_-|$  by multiplying by the complex conjugate and using a Taylor series to give

$$|A_+| = 1 + \frac{\omega^4\Delta t^4}{4} \quad (4.15)$$

$$|A_-| = \frac{i\omega\Delta t}{2} - \frac{i\omega^3\Delta t^3}{2} \quad (4.16)$$

The amplitude error is dependent on the time step and the angular frequency. When  $|A| = 1$  then the scheme is neutral. If  $|A| > 1$  it is amplifying and if  $|A| < 1$  it is damping. The amplitude errors are defined as the difference in modulus between

the amplification factor  $|A|$  and the correct value [2].

The exact solution to equation 4.5 is

$$F(t) = F(0) \exp(i\omega\Delta t) \quad (4.17)$$

with an amplification factor of

$$|A_{\text{exact}}| = \exp(i\omega\Delta t) \quad (4.18)$$

As we increase the numerical resolution by making  $\Delta t \rightarrow 0$  then  $|A_+| \rightarrow 1$ ,  $|A_-| \rightarrow 0$  and  $|A_{\text{exact}}| \rightarrow 1$ . Therefore the second-order Adams-Bashforth method dampens the computational mode.

However, it is not just amplitude errors that arise from the oscillation equation but phase speed errors also. The combining of the amplitude error and phase speed error make up the total error for the scheme. This is an area that can reviewed in the future.

## 4.4 Combined Leapfrog and Forward Step

We have so far implemented a leapfrog with a Robert-Asselin filter and a first-order Adams-Bashforth method separately.

We will now combine the leapfrog scheme and a simple forward scheme to see the affects from the nonlinear model. Figure 4.13 shows the ratio of  $N - 1$  leapfrogs to 1 forward step. When  $N = 2$  this means 1 leapfrog followed by 1 forward step. For every even number of leapfrog steps (when  $N$  is odd) the amplitude is further apart but as we increase the number of leapfrog steps whether even or odd, the amplitude is converging. Figure 4.14 shows the final amplitude against  $N$  which clearly shows the converging for large  $N$ . For an odd number of leapfrog steps when  $N = 2, 4, 6, 8, 10 \dots$  the final amplitude remains fairly constant but for an even number of leapfrog steps when  $N = 3, 5, 7, 9 \dots$  the final amplitude is increasing at a decaying rate until  $N$  becomes sufficiently large. By the time  $N$  is of order  $10^2$  the amplitude has converged to its eventual value.

By combining the leapfrog scheme with a forward step, this helps to control the time-splitting instability associated with the leapfrog scheme. The forward-difference step is used to restart leapfrog integrations. This is an easy method to employ but degrades the numerical accuracy of the leapfrog scheme. As we have discovered the first-order Adams-Bashforth method becomes unstable very quickly. Therefore a second or third-order method may be of better use.

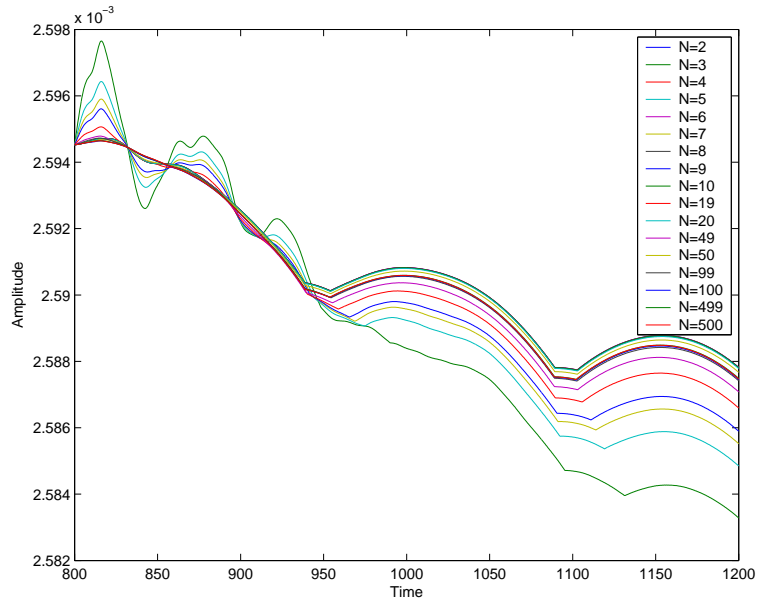


**Figure 4.13:** *Combined leapfrog and forward step.  $N - 1$  leapfrogs to 1 forward step. Shows the amplitude of the perturbation between the two layers in the model.*

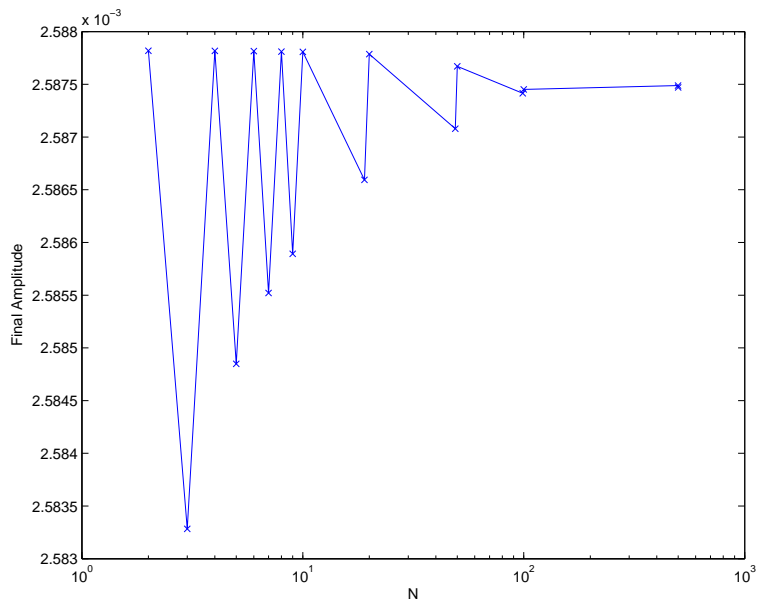


**Figure 4.14:** *Combined leapfrog and forward step. Shows the final amplitude vs  $N$ .*

# Chapter 5

## Sensitivity Tests

In this Chapter we will look at the sensitivity of the schemes we have used in the nonlinear model by varying the time step. We shall also look at the importance of advection, forcing and dissipation in the model.

### 5.1 Changes in $\Delta t$

As mentioned previously the default time step  $\Delta t = 0.0008$ . We have increased  $\Delta t$  and carried out model runs for the three cases of the Asselin-filtered leapfrog scheme. The time step was increased up to a maximum of  $45\Delta t = 0.036$ . Any larger than this then the model would terminate due to the stability of the scheme. As we increase  $\Delta t$  the jump between each time point becomes larger and hence the final amplitude increases up to  $20\Delta t$  but thereafter decreases in amplitude between  $20\Delta t$  and  $30\Delta t$  for each of the three cases. This decrease in amplitude agrees with the linear theory because equation 4.1 dampens the amplitude. Also a time step of  $30\Delta t$  is giving the same amplitude as for  $14\Delta t$ . However, if this is valid then it would be computationally less expensive to run a model with a time step 16 times larger to get the same amplitude.

With the amplitude errors being derived from Taylor series expansions they are only accurate to a certain degree as they are only taken up to the first 3 or 4 terms. Although the magnitude of the remaining terms are smaller they are neglected. After  $30\Delta t$  the amplitude increases further before decreasing after  $40\Delta t$ . It is clear that the nonlinear model is sensitive to time step changes.

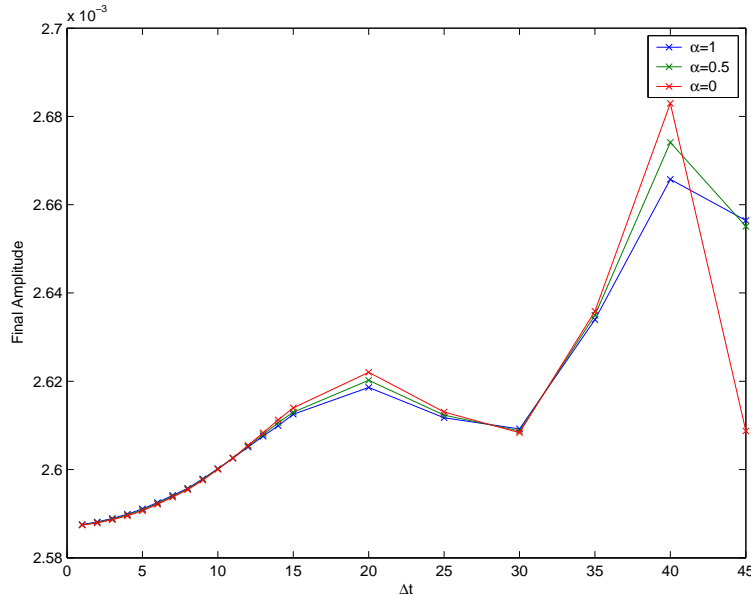


**Figure 5.1:** *Leapfrog scheme with Robert-Asselin filter for the three cases  $\alpha = 1$ ,  $\alpha = 0.5$  and  $\alpha = 0$ . Shows the final amplitude of the perturbation between the two layers in the model for increasing  $\Delta t$ .*

## 5.2 Advection, Forcing and Dissipation

In Chapter 3 we briefly mentioned the forcing, dissipation and advection terms in the model equations.

Here we have included the forcing and dissipation and neglected the advection term for each of the three cases  $\alpha = 1$ ,  $\alpha = 0.5$  and  $\alpha = 0$ . The default time step and filter parameter was applied. Advection is responsible for the movement of fluid parcels from one position to another. Figure 5.2 shows by taking the advection out of the model there is no oscillatory behaviour present. There is strong linear growth with time for each case indicating how important advection is in the model and therefore cannot be neglected. By the end of the integration the amplitude reaches a magnitude of near  $10^{30}$ .

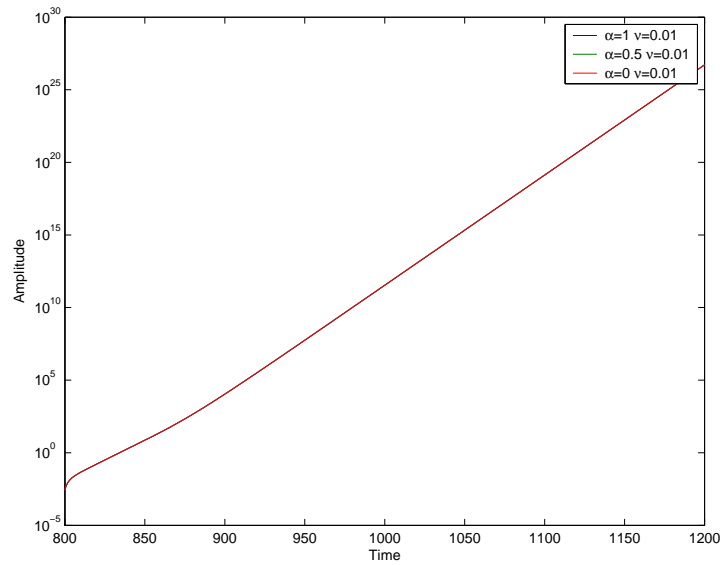


**Figure 5.2:** Leapfrog scheme with Robert-Asselin filter for the three cases  $\alpha = 1$ ,  $\alpha = 0.5$  and  $\alpha = 0$  with a filter parameter  $\nu = 0.01$ . Shows the amplitude of the perturbation between the two layers in the model with no advection. Only forcing and dissipation being applied.

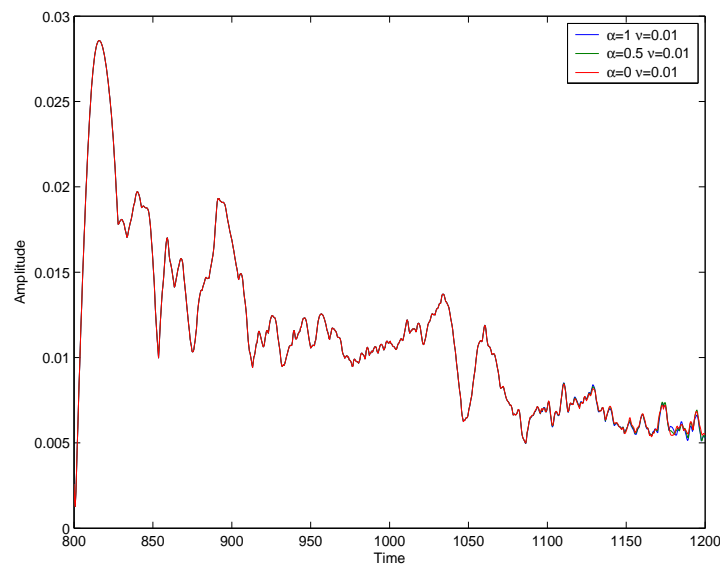


**Figure 5.3:** Leapfrog scheme with Robert-Asselin filter for the three cases  $\alpha = 1$ ,  $\alpha = 0.5$  and  $\alpha = 0$  with a filter parameter  $\nu = 0.01$ . Shows the amplitude of the perturbation between the two layers in the model with no forcing and dissipation. Only advection being applied.

When taking the forcing and dissipation from the model and applying only advection the oscillations become more irregular and the wave amplitudes do not grow as large. Figure 5.3 shows that the amplitudes of the three case of  $\alpha$  perfectly map each other until the final stages of the integration. At this point the phase and amplitudes of the waves begin to deviate.

# Chapter 6

## Conclusion

In this final Chapter we shall conclude the dissertation by summarising the results from the QUAGMIRE v1.3 model from all the different time-differencing schemes used throughout. The benefits and costs of the schemes for NWP models and the future work that needs to be undertaken to take this area of Meteorology to the next level.

### 6.1 Summary

The aim of this dissertation was to implement a number of time-differencing schemes in a simple nonlinear numerical model and compare the time step errors in the schemes with the predictions of simple linear analysis. Then finally deciding whether the schemes could be implemented into existing NWP models.

We have implemented a number of time-differencing schemes into the nonlinear QUAGMIRE v1.3 model. The development of baroclinic waves in the model indicate a good resemblance between the model and laboratory. This indicates that the numerical schemes we have used are reliable.

The first was the leapfrog with Robert-Asselin filter as this is widely used in numerical models and was the default scheme in the nonlinear model. The amplitude error for this scheme (equation 4.1) suggest that the amplitude should decrease as the filter parameter  $\nu$  increases. However, the nonlinear model shows the amplitude increasing and disagreeing with the linear theory for this scheme. From this, it is important to choose a suitable filter parameter. The proposed modified filter [7]

was then tested for the three cases of  $\alpha = 1$ ,  $\alpha = 0.5$  and  $\alpha = 0$ . When  $\alpha = 1$ , this yields the standard filter. When  $\alpha = 0.5$  because you are displacing two points rather than one the scheme is significantly more accurate. When  $\alpha = 0$  the scheme becomes unstable as  $\nu > 0.7$  and the amplitude decreases. The case when  $\alpha = 0.5$  yields third order accuracy and conserves the three-time-level mean state.

Having considered this, we decided to investigate the Adams-Bashforth family of schemes. The first-order Adams-Bashforth method becomes unstable very quickly as the nonlinear model allows baroclinic waves to develop which amplify exponentially due to the amplitude error  $|A| \gg 1$ . The second-order Adams-Bashforth method was found to agree with the linear theory. For increasing  $\Delta t$  the final amplitude increases as  $|A| > 1$  which mean the wave is amplifying. However, the third-order Adams-Bashforth method was found to disagree with the linear theory because for increasing  $\Delta t$  the final amplitude increases also. The amplification factor  $|A| < 1$  which means it should be decaying.

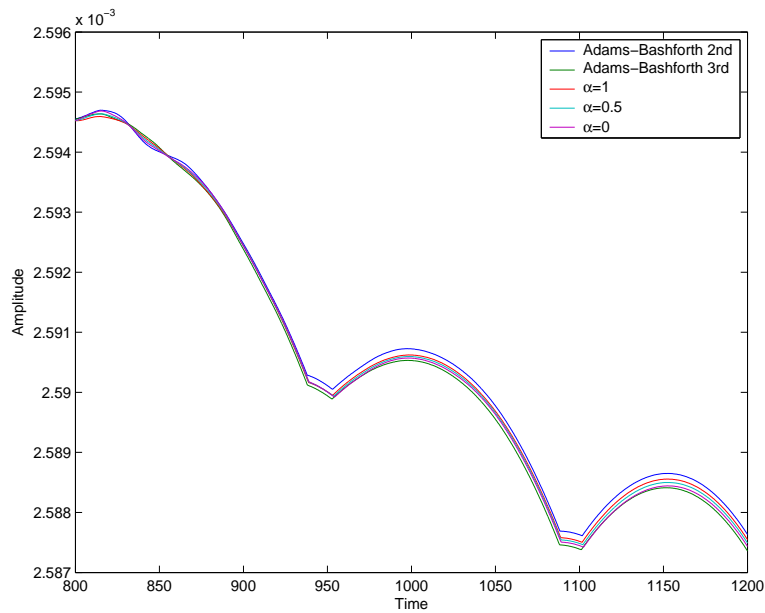


**Figure 6.1:** Shows the comparison of the results from the Adams-Bashforth second-order, Adams-Bashforth third-order and the leapfrog scheme with Robert-Asselin filter for the three cases of  $\alpha$ . Shows the amplitude of the perturbation between the two layers in the model for  $\Delta t = 0.0008$ .

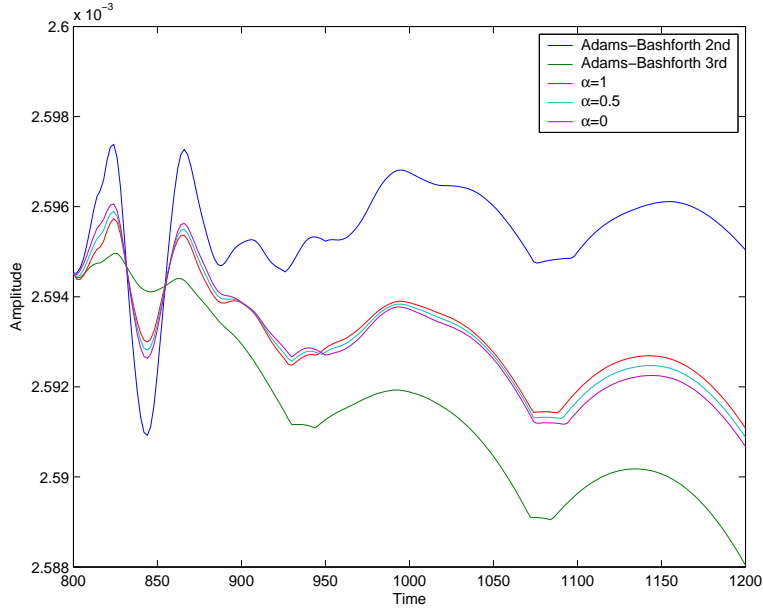


**Figure 6.2:** Shows the comparison of the results from the Adams-Bashforth second order, Adams-Bashforth third order and the leapfrog scheme with Robert-Asselin filter for the three cases of  $\alpha$ . Shows the amplitude of the perturbation between the two layers in the model for  $5\Delta t$ .

Figure 6.1 summarises the results for the three cases of  $\alpha = 1$ ,  $\alpha = 0.5$ ,  $\alpha = 0$  and the second and third-order Adams-Bashforth methods. Using the default time step and default filter parameter the schemes in the model produce similar wave amplitudes. Figure 6.2 shows for larger  $\Delta t$  the second and third-order schemes are more time step dependent. All the schemes suffer from ringing during the initial integrations for larger  $\Delta t$ .

From the selection of time-differencing schemes employed in the model, not surprisingly, the third-order Adams-Bashforth method is more accurate than the Asselin-filtered leapfrog scheme for the  $\alpha = 1$  case and amplitude errors are considerably smaller. However, the Asselin-filtered leapfrog scheme is subject to time-splitting instability, therefore by using a third-order Adams-Bashforth method you can avoid this. The Asselin-filtered leapfrog scheme for  $\alpha = 0.5$  yields third-order accuracy the same as the third-order Adams-Bashforth method. Therefore the proposed modification [7] needs to be given serious thought. The positives to take here are undone by the large phase error with the leapfrog scheme.

## 6.2 Future Work

In the future it would be beneficial to implement and employ more time-differencing schemes into the QUAGMIRE v1.3 model to understand a wider concept of possible schemes that could be used in NWP models. Above all, not every scheme will be perfect, but by analysing the benefits and costs of the schemes it may be possible to determine if the scheme should and could be employed into existing models. If the benefits outweigh the costs then it may be worth implementing. A focus on higher order schemes such as the fourth-order Runge-Kutta could be looked at. The length of the time integration could be extended with more computer power and faster simulations given the time constraints. Further improvements to QUAGMIRE v1.3 in the source code as well as diagnostics by considering a multilayer model instead of the current two-layer model of equal resting depth.

## Bibliography

- [1] Asselin, R., (1972): Frequency filter for time integrations. *Mon. Wea. Rev*, **100**, 487–490.
- [2] Durran, D.R., (1999): *Numerical Methods for Wave Equations in Geophysical Fluid Dynamics*. Springer-Verlag.
- [3] Durran, D. R., (1991): The third-order AdamsBashforth method: An Attractive Alternative to Leapfrog Time Differencing. *Mon. Wea. Rev*, **119**, 702–720.
- [4] Pedlosky, J., (1979): *Geophysical Fluid Dynamics*. Springer-Verlag.
- [5] Pfeffer, R., I. Navon, and X. Zou., (1992): A comparison of the impact of two time-differencing schemes on the NASA GLAS climate model. *Mon. Wea. Rev*, **120**, 1381–1393.
- [6] Robert, A.J., (1966): The integration of a low-order spectral form of the primitive meteorological equations. *J. Meteor. Soc. Japan*, **44**, 237–244.
- [7] Williams, P.D., (2009): A proposed modification to the Robert-Asselin time filter. *Mon. Wea. Rev*, **137**, 2538–2546.
- [8] Williams, P.D., T.W.N.Haine, P.L.Read, S.R.Lewis and Y.H.Yamazaki., (2009): QUAGMIRE v1.3: A quasi-geostrophic model for investigating rotating fluid experiments. *Geosci. Model Dev*, **2**, 13–32.
- [9] Zhao.B and Zhong.Q., (2009): The Dynamical and Climate Tests of an Atmospheric General Circulation Model Using the Second-Order Adams-Bashford Method. *Acta Meteor. Sinica*, **23**, 738–749.